The three-dimensional structure of flexible resorcinol-formaldehyde aerogels investigated by means of holotomography

René Tannert[*,1], Marina Schwan[1], Ameya Rege[2], Mario Eggeler[1], Julio Cesar da Silva[3], Marion Bartsch[1], Barbara Milow[1], Mikhail Itskov[2], and Lorenz Ratke[1]

[1]Institute of Materials Research, German Aerospace Center, Linder Höhe, 51147 Cologne, Germany

[2]Department of Continuum Mechanics, RWTH Aachen University, Kackertstraße 9, 52072 Aachen, Germany

[3]European Synchrotron Research Facility (ESRF), 38000 Grenoble, France

René Tannert
telephone +49 2203 6014291
fax: +49 2203 68936
email: rene.tannert@dlr.de

Abstract

Organic aerogels based on resorcinol-formaldehyde (RF) gels display remarkable properties due to their pronounced nanoporosity. Therefore, studies towards the understanding of their structure-property-relationship are of high value for the design of improved materials. X-ray tomography is a technique that has been used for the structural elucidation of porous materials, but so far no highly resolved three-dimensional structures of RF gels have been obtained under the classical absorption-based experimental X-ray setup. This paper reports on the successful analysis of a superflexible RF aerogel (sf-RF) using zoom holotomography that yielded images with an unprecedented resolution in the sub-micrometer range. The preparation of suitable powder from monolithic sf-RF, the experimental conditions for tomography, and data-processing to obtain a 3D-image of the dried gel sample are described.

Macropores above ca. 75 nm could be identified and visualized. They were shown to adopt almost spherical shape and to display a low connectivity. A quantitative analysis of the pore space revealed that most of the identified pores are small macropores (diameter < 0.5 µm), yet most pore volume is located in larger macropores of 1 - 4 µm diameter.

Graphical abstract

Keywords

aerogels - 3D-structure - holotomography - pore-size distribution

Acknowledgments

The authors wish to thank Benjamin Ignatzi for the production and characterization of powders and Guillermo Requena and Galina Kasperovich for assistance and computer resources provided during preliminary image analysis. We thank the European Synchrotron Radiation Facility for access to synchrotron radiation facilities at ID16A beamline (proposal SC4154 granted to R.T., M.S., A.R., B.M., M. I., and L.R.). Financial support from the German Aerospace Center (program “Terrestrial vehicles”, project “Next Generation Car” for R.T., M.S., B.M., and L.R.) is gratefully acknowledged.

1 Introduction

Aerogels are nanostructured open-porous materials with a very low density that renders them excellent materials for thermal insulation purposes [1]. The gel structure can be suitably tailored by adjustment of chemical

parameters during synthesis (concentration of reagents, pH value). Among all aerogels, organic gels based on resorcinol-formaldehyde (RF gels) play a prominent role as they show the lowest thermal conductivity determined so far [2]. In order to improve the thermal, mechanical, and other properties an in-depth knowledge of the three-dimensional (3D) structure of aerogels is a prerequisite as it allows modeling and simulation studies [3,4]. To this end, the porous nature of aerogels is most commonly assessed quantitatively using methods that rely on (nitrogen) sorption [5]. However, methods used to determine the pore-size distribution are limited by underlying assumptions - the popular Barrett-Joyner-Halenda (BJH) model, for instance, involves a cylindrical pore shape and does not give information about the full range of pore-width and volume [6]. Although data on porosity obtained via the BJH model have yielded multi-scale mechanical models of aerogels based on silica [7] and cellulose [8], the exploitation of modeling tools is still limited by such simplified pore models. Alternative computational methods that combine density functional theory calculations and sorption experiments, although established for several classes of rigid, ordered porous solids, cannot be confidently applied to aerogels as their porous network undergoes deformation upon adsorption [9,10].

Another common method that can provide pore-size distributions over a large range (from a few nm to micrometer) is mercury porosimetry [11]. It is, however, only reliable for very stiff aerogels as more flexible samples can be significantly compressed during the intrusion experiment [12,13].

Electron microscopy is well-established as a tool to provide two-dimensional (2D) images of aerogels on the nanometer scale [5]. A combination of focused ion beam milling and scanning electron microscopy has proven to represent a powerful technique to obtain highly resolved 3D structures of porous materials [14,15]. Although it has been successfully applied to mesoporous carbon [16-18], it has not yet been used to provide 3D images of RF gels, since they are more difficult to investigate due to a rapid electric charging during measurements hampering suitable image detection.

Tomographic methods that use X-ray irradiation have been used to visualize porous materials such as metal foams [19], and also some low resolution 3D-structural images of composite materials containing RF gels have been described [20,21]. However, RF gels are rapidly destroyed in the classical experimental setup of X-ray absorption when higher energy levels are used. Thus, no 3D-nanostructure has yet been extracted from X-ray absorption experiments. In that context, nanoscale zoom holotomography provides an alternative X-ray imaging method that does not rely on absorption, but instead on the phase-contrast [22]. Holotomography is capable of imaging materials with a high sensitivity for electron density, high isotropic spatial resolution (down to ~30 nm) and small voxel size (down to ~5nm). As very light materials (such as aerogels) do not absorb much of the X-rays, the phase-contrast image plays a key role to efficiently visualize and quantify pore geometries. This technique has already been successfully applied to the structural elucidation of porous systems including Metal Matrix Composites [23,24], Solid Oxide Fuel Cell electrodes [25,26], and Arabidopsis seeds [27].

Aerogels have not been studied using holotomography, and our article describes efforts to this end. For first tests, superflexible resorcinol-formaldehyde (sf-RF) gels were selected [28], as they possess rather large particles and pores in the sub-micrometer range. They should be easier to visualize than classical Pekala-type RF aerogels which have both particles and pores in the low nanometer range [29].

2 Experimental setup

2.1 Preparation and characterization of RF aerogel samples

Monoliths of sf-RF aerogels were synthesized and dried using supercritical carbon dioxide as reported previously [28]. Aerogel monoliths were ground with a planetary micro mill (Pulverisette 7, Fritsch, Germany) filled with 17 zirconium oxide balls (of approximately 10 mm diameter). For grinding the mill was sealed and rotated for 7 minutes at a velocity of 700 rpm. The milling process was repeated three times with 3 minutes cooling interval in-between milling cycles. The envelope density of monolithic sf-RF was calculated from measured volume and weight of an aerogel piece, whereas the envelope density of sf-RF powder was measured with a GeoPyc 1360 analyzer (Micromeritics, USA). The skeletal density was measured by helium pycnometry

using an AccuPyc machine (Micromeritics, USA). The internal surface area of the aerogel monolith and powder was calculated from the nitrogen adsorption-desorption isotherms measured on a TriStarII machine (Micromeritics, USA) using the method from Brunauer, Emmett, and Teller (BET, [30]) implemented in the Micromeritics software. Before analysis, the samples were outgassed for 6 hours at 110°C and 10^{-2} mbar. The microstructure of the aerogels was investigated using a Merlin scanning electron microscope (SEM; Zeiss, Germany). RF aerogels, which are electrically non-conductive, were coated with gold prior to SEM. The average particle diameter was determined by applying the linear intercept method on SEM images [31]. This method, which was originally developed for metals and alloys, can be adapted to aerogels as long as they possess a particulate structure. Light microscopy was performed using a SteREO Discovery.V12 stereomicroscope (Zeiss, Germany). Mercury porosimetry (conducted by Porotec, Germany) failed to produce reliable intrusion data due to substantial deformation of the sample during the experiment.

2.2 Preparation of the sample for nanoholotomography

Thin-walled quartz glass capillaries of 100 µm outer diameter and 10 µm wall thickness (Hilgenberg, Germany) were densely filled with aerogel powder dried in an oven at 120 °C and ambient pressure over night. Subsequently, the capillary was cut to 10-15 mm length, hermetically sealed with paraffin wax, and fixed with Loctite Super Glue 3® onto sample holders for nanotomography (see Figure 1).

[Figure 1: Aerogel-filled glass capillary glued onto the sample holder (a) and magnified view on the glass capillary (b)]

2.3 Nanoscale zoom holotomographic analysis on sf-RF aerogels

The holotomography experiments were performed at the ID16A Nano-Imaging beamline recently built at ESRF, Grenoble [32,26]. The 17.05 keV X-ray beam was nano-focused using Kirkpatrick-Baez mirrors to a spot size of about 30 nm, and the magnified projections of the samples were recorded by a FReLoN detector [33]. The scans were carried out using the zoom tomography approach where the samples of sf-RF aerogel were imaged at four different focus-to-sample distances [22,26]: 24.160 mm, 25.197 mm, 29.343 mm and 37.951 mm. Such distances were chosen to achieve an effective voxel size of 60 nm. 2000 projections were acquired over 180 degrees for each distance. The focus-to-detector distance was 1.2 m. A total of 8000 projections were therefore acquired with exposure time of 1s which took about 4 h to complete. The experiments were performed at room temperature.

2.4 Three-dimensional reconstruction

The obtained holotomographic projections are phase contrast images taken at the holographic regime. Using the Fresnel fringes on the images at the four distances with different magnifications, it is possible to recover the phase-shifts due to the specimen [22]. Such phase maps are proportional to the projection of the electron density of the material. First, the projections are rescaled down to the smallest pixel dimension recorded during the scan, and then, the projections recorded at four distances are aligned. The phase retrieval at each tomographic angle, as described in a previous work by Cloetens and coworkers [34], was carried out with in-house software using the GNU Octave programming environment (http://www.octave.org) and the public domain image analysis program ImageJ (http://rsbweb.nih.gov/ij/). The 3D volumes were reconstructed from the phase maps using the filtered back-projection (FBP) [35] with the ESRF software PyHST. The resulting volume contained 2048 x 2048 x 2048 pixels.

2.5 Image analysis

The raw volume was visualized and analyzed using the “Avizo” software package (version 9.2; FEI Company, Hillsboro, United States). The extracted subvolume was filtered with an edge-preserving smoothing image filter (Bilateral filter) in order to reduce noise and to facilitate generating a binary image for separating macropores

and denser material. A 2D- and 3D-threshold preview was used to set the lower and upper threshold interval of the "Interactive Thresholding" module in Avizo. Different threshold values were tried resulting in different computed material porosity and size and numbers of macropores. A threshold interval ranging from -1200 to 110 was chosen for further analysis assuring that all macropores are captured and pores are not connected to each other. Even though some pores might be connected, this selected threshold data should provide a reasonable assumption for macropore-size distribution. The "Volume Fraction" and "Label Analysis" tools in Avizo were then used for the determination of the material porosity and labelling of each pore, respectively. Furthermore, different colors were assigned to independent pores.

3 Results and Discussion

A first issue was to produce aerogel powder grains small enough to enter the microcapillary envisioned for the tomography experiment, yet large enough to retain the microstructure including pores. To this end, we employed a planetary ball mill and compared several properties of monolith and powder [36]. As indicated in table 1, the inner surface area (BET area), the envelope (ρ_e) and the skeletal (ρ_s) densities, as well as the resulting porosity of the monolith and the powder matched well which indicates that there is no alteration of the microstructure. Also, scanning electron micrographs show no significant change in the microstructure (Fig. 2). The microstructural analysis of both aerogel monolith and powder revealed an average particle size of about 0.11 µm, while large pores in the range of 2-7 µm were observed. Since the monolith and the powder display similar structure and properties, the powder appears to be a viable surrogate for the monolithic sf-RF and was thus employed in tomography.

Table 1: Properties of sf-RF aerogel determined for monolith and powder

Sample	**BET, m^2/g**	**ρ_e, g/cm^3**	**ρ_s, g/cm^3**	**Porosity[a], %**
sf-RF monolith	52	0.0650	1.53	95.8
sf-RF powder	45	0.0623	1.47	95.8

[a]the porosity was calculated from envelope and skeletal densities [37]

[Figure 2: Microstructure of monolithic (a) and powdered (b) sf-RF samples]

Figure 3 shows the reconstructed 3D structure obtained by X-ray holotomography. Three orthogonal slices are displayed, and a small cubic region is highlighted to give an idea of scale. In a first qualitative interpretation, such a 3D representation suggests a higher density of material between the powder grains which was puzzling since those regions should have been filled only with air and thus should appear darker than the solid material. A possible explanation of this phenomenon is that upon milling loose sf-RF particles may have been accumulated between the highly porous grains leading to a higher material density outside the grains than inside.

[Figure 3: tomogram of sf-RF aerogel; a representative region of interest was selected from a RF grain (red bounding box with cube edge length of 1.5 µm)]

Within a bigger grain of sf-RF a cubic region of interest with edge length of 1.5 µm was selected for further analysis (red bounding box in figure 3, figure 4a). The extracted subvolume was binarized in order to distinguish between material and macropores. As this binarization step was in particular prone to give biased results, care was taken to identify pores unequivocally by only selecting areas with sharp decrease in gray-values as pores (see Figure 4b). Pores identified in this way were then analyzed with respect to the pore diameter and volume.

[Figure 4: Image of extracted subvolume after applying bilateral filter (a); pores identified are highlighted in blue (b)]

In total, 1056 macropores with volumes ranging from $2.16 \cdot 10^{-4}$ µm^3 (volume of one voxel) to 51.7 µm^3 were identified and labeled (Figure 4). A rather low material porosity of 14.8 % was computed using volume fraction analysis. The huge difference in porosity as computed from 3D x-ray data to porosity values that were determined using pycnometry (96 %, see table 1) may be mainly attributed to the presence of mesopores and very small macropores that were out of reach for our experimental setting. An analogous experiment using a voxel size of 30 nm in local tomography mode did not yield a useful 3D reconstruction for sf-RF. Since the field-of-view is smaller in that setting, all material surrounding the field-of-view contribute as noise to the experiment thus hampering further analysis of the raw data. An alternative sample envisioned for future X-ray experiments could consist of a single aerogel grain that is glued to the sample holder and thus is only surrounded by air.

[Figure 5: Visualization of the pore space (for clarity, colored pores are shown without material)]

A visual inspection of macropores as identified in the region of interest indicated that a spherical geometry might be used to further analyze pores quantitatively (Figure 5). A corresponding analysis shows that the majority of identified pores, with diameters between 74.4 nm and 4.62 µm, are in the low macropore regime (diameters below 0.5 µm) whereas relatively few larger pores (diameter > 1.5 µm) were found (Figure 6a). Most of the macropore volume, however, seems to be located in pores of 1 to 4 µm diameter as suggested by the bimodal distribution of relative pore-volume illustrated in Figure 6b. As pore-sizes and corresponding volumes affect the kinetic profiles of transport processes taking place in the aerogel, these findings might have implications for the use of RF gels, for instance as matrix for metals in catalysis [38] or as carrier of metal-organic frameworks for sorptive applications [39]. Furthermore, the structural data obtained so far might be useful for studies towards a modeling of the mechanical and thermal properties of RF-aerogels.

[Figure 6: representations of distributions of the absolute pore-diameter (a; histogram with a class width of 0.2 µm) and the relative pore volume (b)]

4 Conclusions and Outlook

Superflexible resorcinol-formaldehyde aerogels were proven as suitable probes for zoom holotomography. Insights into the 3D structure of such gels could be obtained at the macropore level. For microstructural characterization, macro-porosity was treated as an entity of individual spherical pores. Distributions of both pore size and pore volume were determined. Accordingly, most pores are small macropores (diameter < 0.5 µm) whereas most of the pore volume is located in larger macropores of 1 - 4 µm diameter.

Comparative studies on other aerogel and xerogel samples are ongoing. These include the investigation of more rigid gels in order to validate the pore-size distribution extracted from holotomography using mercury porosimetry. Current efforts are also devoted to the extraction of physical quantities for the description of pore shape (e.g. Feret diameters) and connectivity (Euler numbers) and will be published in due course. Further X-ray holotomographic experiments are planned using smaller samples that might allow for the use of smaller voxel sizes and, consequently, for structural data at higher spatial resolution that also allow to investigate the mesopore regime.

References

1. Aegerter MA, Leventis N, Koebel MM (eds) (2011) Aerogels Handbook. Springer New York,
2. Lu X, Arduini-Schuster MC, Kuhn J, Nilsson O, Fricke J, Pekala RW (1992) Thermal Conductivity of Monolithic Organic Aerogels. Science 255 (5047):971-972

3. Pekala RW, Alviso CT, LeMay JD (1990) Organic aerogels: microstructural dependence of mechanical properties in compression. J Non-Cryst Solids 125 (1–2):67-75
4. Lu X, Caps R, Fricke J, Alviso CT, Pekala RW (1995) Correlation between structure and thermal conductivity of organic aerogels. J Non-Cryst Solids 188 (3):226-234
5. Reichenauer G (2011) Structural Characterization of Aerogels. In: Aegerter MA, Leventis N, Koebel MM (eds) Aerogels Handbook. Springer New York, New York, pp 449-498
6. Barrett EP, Joyner LG, Halenda PP (1951) The Determination of Pore Volume and Area Distributions in Porous Substances. I. Computations from Nitrogen Isotherms. J Am Chem Soc 73 (1):373-380
7. Fu B, Luo H, Wang F, Churu G, Chu KT, Hanan JC, Sotiriou-Leventis C, Leventis N, Lu H (2011) Simulation of the microstructural evolution of a polymer crosslinked templated silica aerogel under high-strain-rate compression. J Non-Cryst Solids 357 (10):2063-2074
8. Rege A, Schestakow M, Karadagli I, Ratke L, Itskov M (2016) Micro-mechanical modelling of cellulose aerogels from molten salt hydrates. Soft Matter 12 (34):7079-7088
9. Reichenauer G, Scherer GW (2000) Nitrogen adsorption in compliant materials. J Non-Cryst Solids 277 (2–3):162-172
10. Landers J, Gor GY, Neimark AV (2013) Density functional theory methods for characterization of porous materials. Colloids Surf, A 437:3-32
11. Giesche H (2006) Mercury Porosimetry: A General (Practical) Overview. Part Part Syst Charact 23 (1):9-19
12. Johnston GP, Smith DM, Melendez I, Hurd AJ (1990) Compression effects in mercury porosimetry. Powder Technol 61 (3):289-294
13. Scherer GW, Smith DM, Stein D (1995) Deformation of aerogels during characterization. J Non-Cryst Solids 186 (0):309-315
14. Holzer L, Indutnyi F, Gasser PH, Münch B, Wegmann M (2004) Three-dimensional analysis of porous BaTiO3 ceramics using FIB nanotomography. J Microsc (Oxford, U K) 216 (1):84-95
15. Wilson JR, Kobsiriphat W, Mendoza R, Chen H-Y, Hiller JM, Miller DJ, Thornton K, Voorhees PW, Adler SB, Barnett SA (2006) Three-dimensional reconstruction of a solid-oxide fuel-cell anode. Nat Mater 5 (7):541-544
16. Ziegler C, Thiele S, Zengerle R (2011) Direct three-dimensional reconstruction of a nanoporous catalyst layer for a polymer electrolyte fuel cell. J Power Sources 196 (4):2094-2097
17. Balach J, Miguel F, Soldera F, Acevedo DF, Mücklich F, Barbero CA (2012) A direct and quantitative image of the internal nanostructure of nonordered porous monolithic carbon using FIB nanotomography. J Microsc (Oxford, U K) 246 (3):274-278
18. Balach J, Soldera F, Acevedo DF, Mücklich F, Barbero CA (2013) A Direct and Quantitative Three-Dimensional Reconstruction of the Internal Structure of Disordered Mesoporous Carbon with Tailored Pore Size. Microsc Microanal 19 (3):745-750
19. Maire E (2012) X-Ray Tomography Applied to the Characterization of Highly Porous Materials. Annu Rev Mater Res 42 (1):163-178
20. Haghgoo M, Plougonven E, Yousefi AA, Pirard J-P, Léonard A, Job N (2012) Use of X-ray microtomography to study the homogeneity of carbon nanotube aqueous suspensions and carbon nanotube/polymer composites. Carbon 50 (4):1703-1706
21. Laskowski J (2016) Synthese und Eigenschaften von Aerogel-Aerogel-Verbundwerkstoffen. Dissertation / PhD Thesis, Rheinisch-Westfälische Technische Hochschule Aachen, Aachen
22. Mokso R, Cloetens P, Maire E, Ludwig W, Buffière J-Y (2007) Nanoscale zoom tomography with hard x rays using Kirkpatrick-Baez optics. Appl Phys Lett 90 (14):144104
23. Kenesei P, Biermann H, Borbély A (2005) Structure–property relationship in particle reinforced metal–matrix composites based on holotomography. Scr Mater 53 (7):787-791
24. Girardin E, Renghini C, Dyson J, Calbucci V, Moroncini F, Albertini G (2011) Characterization of Porosity in a Laser Sintered MMCp Using X-Ray Synchrotron Phase Contrast Microtomography. Mater Sci Appl 2:1322-1330
25. Sar J, Celikbilek O, Villanova J, Dessemond L, Martin CL, Djurado E (2015) Three dimensional analysis of Ce0.9Gd0.1O1.95–La0.6Sr0.4Co0.2Fe0.8O3−δ oxygen electrode for solid oxide cells. J Eur Ceram Soc 35 (16):4497-4505
26. Hubert M, Laurencin J, Cloetens P, da Silva JC, Lefebvre-Joud F, Bleuet P, Nakajo A, Siebert E (2016) Role of microstructure on electrode operating mechanisms for mixed ionic electronic conductors: From synchrotron-based 3D reconstruction to electrochemical modeling. Solid State Ionics 294:90-107
27. Cloetens P, Mache R, Schlenker M, Lerbs-Mache S (2006) Quantitative phase tomography of Arabidopsis seeds reveals intercellular void network. Proc Natl Acad Sci U S A 103 (39):14626-14630
28. Schwan M, Tannert R, Ratke L (2016) New soft and spongy resorcinol–formaldehyde aerogels. J Supercrit Fluids 107:201-208
29. Pekala RW, Kong FM (1989) A Synthetic Route To Organic Aerogels - Mechanism, Structure, and Properties. J Phys 50 (C-4):C433-C440

30. Brunauer S, Emmett PH, Teller E (1938) Adsorption of Gases in Multimolecular Layers. J Am Chem Soc 60 (2):309-319
31. Heyn E (1903) Short reports from the metallurgical laboratory of the royal mechanical and testing institute of Charlottenburg. The Metallographist 6:39-70
32. Zabler S, Cloetens P, Guigay J-P, Baruchel J, Schlenker M (2005) Optimization of phase contrast imaging using hard x rays. Rev Sci Instrum 76 (7):073705
33. Labiche J-C, Mathon O, Pascarelli S, Newton MA, Ferre GG, Curfs C, Vaughan G, Homs A, Carreiras DF (2007) Invited article: The fast readout low noise camera as a versatile x-ray detector for time resolved dispersive extended x-ray absorption fine structure and diffraction studies of dynamic problems in materials science, chemistry, and catalysis. Rev Sci Instrum 78 (9):091301
34. Cloetens P, Ludwig W, Baruchel J, Van Dyck D, Van Landuyt J, Guigay JP, Schlenker M (1999) Holotomography: Quantitative phase tomography with micrometer resolution using hard synchrotron radiation x rays. Appl Phys Lett 75 (19):2912-2914
35. Bracewell RN, Riddle AC (1967) Inversion of fan-beam scans in radio astronomy. Astron J 150 (2):427-434
36. Piedboeuf M-LC, Léonard AF, Traina K, Job N (2015) Influence of the textural parameters of resorcinol–formaldehyde dry polymers and carbon xerogels on particle sizes upon mechanical milling. Colloids Surf, A 471:124-132
37. Tannert R, Schwan M, Ratke L (2015) Reduction of shrinkage and brittleness for resorcinol-formaldehyde aerogels by means of a pH-controlled sol–gel process. J Supercrit Fluids 106:57-61
38. Moreno-Castilla C, Carrasco-Marín F, Dawidziuk M (2012) Carbon Aerogel-Supported Pt Catalysts for the Hydrogenolysis and Isomerization of n-Butane: Influence of the Carbonization Temperature of the Support and Pt Particle Size. Catalysts 2 (4):422
39. Wickenheisser M, Herbst A, Tannert R, Milow B, Janiak C (2015) Hierarchical MOF-xerogel monolith composites from embedding MIL-100(Fe,Cr) and MIL-101(Cr) in resorcinol-formaldehyde xerogels for water adsorption applications. Micropor Mesopor Mater 215 (0):143-153

Fig 1a

Fig 1b

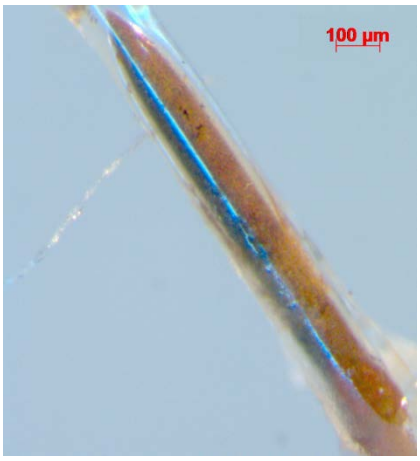

Fig 2a

Fig 2b

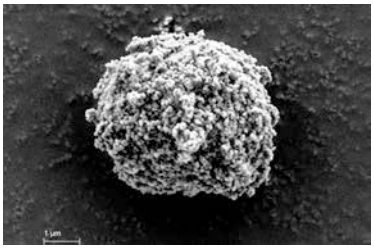

Fig 3

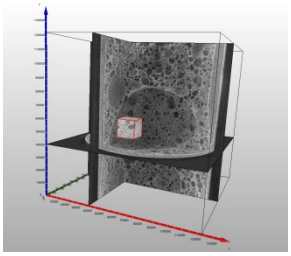

Fig 4a

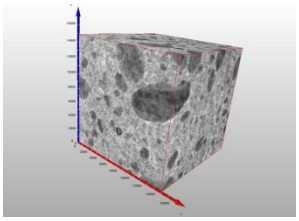

Fig 4b

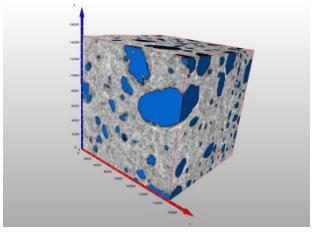

Fig5

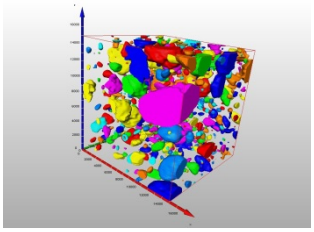

Fig 6a

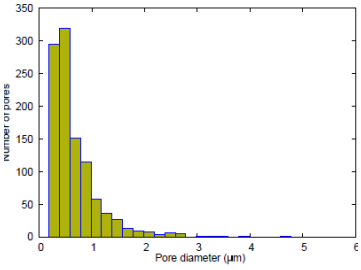

Fig 6b